Available online at www.sciencedirect.com
ScienceDirect
Biochimica et Biophysica Acta 1768 (2007) 1526–1540
Biochimica et Biophysica Acta BBA
www.elsevier.com/locate/bbamem

Galactosyl headgroup interactions control the molecular packing of wheat lipids in Langmuir films and in hydrated liquid-crystalline mesophases

C. Bottier [a], J. Géan [b], F. Artzner [a], B. Desbat [b], M. Pézolet [c], A. Renault [a], D. Marion [d], V. Vié [a,*]

[a] Groupe Matière Condensée et Matériaux, UMR CNRS 6626, Université Rennes I, Campus Beaulieu, Rennes, France
[b] Laboratoire de Physico-Chimie Moléculaire, UMR CNRS 5803, Université Bordeaux I, Talence, France
[c] Département de Chimie, Centre de Recherche en Sciences et Ingénierie des Macromolécules, Université Laval, Québec, Canada G1K 7P4
[d] Unité de Recherche Biopolymères, Interactions et Assemblages, Institut National de la Recherche Agronomique, BP71627, Nantes cedex 3, France

Received 22 November 2006; received in revised form 19 February 2007; accepted 21 February 2007
Available online 13 March 2007

Abstract

The behavior of the two major galactolipids of wheat endosperm, mono- (MGDG) and di-galactosyldiacylglycerol (DGDG) was studied in aqueous dispersion and at the air/liquid interface. The acyl chains of the pure galactolipids and their binary equimolar mixture are in the fluid or liquid expanded phase. SAXS measurements on liquid-crystalline mesophases associated with the electron density reconstructions show that the DGDG adopts a lamellar phase L_α with parallel orientation of the headgroups with respect to the plane of the bilayer, whereas MGDG forms an inverse hexagonal phase H_{II} with a specific organization of galactosyl headgroups. The equimolar mixture shows a different behavior from those previously described with formation of an *Im3m* cubic phase. In comparing monolayers composed of the pure galactolipids and their equimolar mixtures, PM-IRRAS spectra show significant differences in the optical properties and orientation of galactosyl groups with respect to the interface. Furthermore, Raman and FTIR spectroscopies show that the acyl chains of the galactolipid mixture are more ordered compared to those of the pure components. These results suggest strong interactions between MGDG and DGDG galactosyl headgroups and these specific physical properties of galactolipids are discussed in relation to their biological interest in wheat seed.

Keywords: Galactolipid; Air/liquid interface; Glycosyl headgroup organization; Small-angle X-ray scattering; Phase behavior; Wheat endosperm

1. Introduction

Compartmentalization of cell metabolism and control of the intra- and extracellular exchanges are managed by lipoprotein membranes organized in a bilayer structure. This bilayer arrangement is driven by the unique associative properties of membrane lipids in the aqueous environment. In most animal and prokaryote cells, phospholipids are the most abundant membrane lipids. Glycolipids are present in all membranes as quantitatively minor components, although they play major roles in the function of membranes, especially in rafts [1]. Unlike animal cells, glycolipids are the major lipids of higher plants. These glycolipids concentrate in plastids, especially chloroplasts, as di-galactosyl and mono-galactosyldiacylglycerol, i.e., DGDG and MGDG. These lipids are concentrated in the thylakoid membrane, the internal membrane system of the chloroplast specialized in the energy transduction process. The equilibrium between DGDG and MGDG contents has a significant impact on the function of thylakoid membrane proteins, especially that of the light harvesting complexes of the photosystem [2]. These galactolipids are also involved in the targeting of proteins to and within the chloroplast [3] as in the generation of lipid signaling molecules [4,5]. Due to the biological importance of galactolipids in photosynthesis, numerous studies have been performed on the physico-chemical properties

Abbreviations: AFM, atomic force microscopy; ATR, attenuated total reflectance; CPK, Corey–Pauling–Koltun; DGDG, 1,2-di-*O*-acyl-3-*O*-(β-D-galactopyranosyl-1,6-β-D-galactopyranosyl)-*sn*-glycerol; DMPC, 1,2-di-myristoyl-3-phosphorylcholine-*sn*-glycerol; DOPC, 1,2-di-oleoyl-3-phosphorylcholine-*sn*-glycerol; FT-IR, Fourier transform infrared spectroscopy; LB film, Langmuir–Blodgett film; MGDG, 1,2-di-*O*-acyl-3-*O*-(β-D-galactopyranosyl)-*sn*-glycerol; PM-IRRAS, polarization modulation-infrared reflexion-absorption spectroscopy; SAXS, small-angle X-ray scattering; WAXS, wide-angle X-ray scattering

* Corresponding author. GMCM, Bât. 11A, Campus Beaulieu, Université Rennes 1. Tel.: +33 2 23 23 56 45; fax: +33 2 23 23 67 17.
E-mail address: veronique.vie@univ-rennes1.fr (V. Vié).

0005-2736/$ - see front matter © 2007 Elsevier B.V. All rights reserved.
doi:10.1016/j.bbamem.2007.02.021

of these unusual polar lipids. Particularly, the phase behavior of chloroplast galactolipids, i.e., their liquid-crystalline packing properties in aqueous solvent, has been thoroughly investigated. While DGDG forms bilayers, i.e., lamellar liquid-crystalline structures (L_α), MGDG molecules aggregate in inverted rod-like structures of infinite length packed in hexagonal arrays, the so-called hexagonal type-II (H_{II}) structure [6]. Non-bilayer lipids such as MGDG may serve to drive the formation of lipoprotein stacks in thylakoid membranes [7]. DGDG and MGDG are also present in non-photosynthetic plant organs and are, for example, the major membrane lipids of the amyloplast [8]. While most of the research effort has been expended in understanding the role of galactolipids in the photosynthetic apparatus, few studies have focused on the role of these galactolipids in the plastids of non-photosynthetic plant organs, i.e., seeds, tubers and roots. These plastids play a central role in the synthesis and storage of different products including pigments, starch and lipids, and it could be expected that the lipid composition of their envelopes regulates the storage function. The amyloplast galactolipids differ mainly from the corresponding chloroplast lipids in their fatty acid composition. Thus, while amyloplast galactolipids are rich in linoleic acid, i.e., an octadecadienoic fatty acid, the galactolipids of chloroplast concentrate linolenic acid, i.e., an octadecatrienoic fatty acid. This difference may have an impact on the general shape of galactolipids, a parameter that is closely related to the liquid-crystalline properties of polar lipids [9]. However, preliminary studies have indicated that isolated amyloplast galactolipids have a similar molecular shape to those found in chloroplasts [10]. Finally, the liquid-crystalline properties of MGDG in aqueous solutions resemble those of phosphatidylethanolamine (PE) where unsaturated MGDG and PE form hexagonal H_{II} structures while the corresponding saturated lipids form bilayers [9].

In addition to the biological role of galactolipids in the diverse biological function of plastids, they are also involved in technological processing of plant products. As an example, galactolipids are involved in the processing of wheat seeds into flour and baked products. They are involved in gas retention in bread dough by forming stable lipoproteins films at the air/water interfaces [11]. They could also play a role in the close packing of the wheat endosperm which defines the hard (compact) and soft (friable) phenotypes of endosperm from hexaploid wheats and, consequently, their milling properties [12]. Particularly, it has been shown that the lipid deposits found between the protein matrix and starch granules of the dry endosperm of a hard wheat are organized in non-bilayer structures, probably inverted hexagonal and inverted cubic phases [13]. Strikingly, there are close relationships between hardness and extractability of polar lipids with apolar solvents. For example, a negative correlation was found for the non-bilayer forming galactolipid, MGDG, while a positive one was observed for DGDG, the lamellar forming galactolipid [14]. It has been also suggested that the extractability of polar lipids could be influenced by their liquid-crystalline state [11]. Furthermore, hardness is also associated with the adsorption of lipids and unusual lipid binding proteins, i.e., puroindolines, onto the surface of starch granules [12,15]. Puroindolines are capable of insertion into lipid monolayers to form highly aggregated structures [16]. Therefore, the texture of wheat endosperm may be controlled by galactolipids in the liquid-crystalline state, which may depend on particular interactions between galactosyl headgroups.

In regard to the different functions of these unique plant lipids, the associative properties of wheat endosperm MGDG and DGDG have been investigated at air/liquid interfaces and in hydrated liquid-crystalline phases. For this purpose, different complementary physical techniques were employed to investigate the packing properties of wheat galactolipids in monolayers and in hydrated liquid-crystalline phases. In particular, we focused on the physical properties of mixtures of hydrated MGDG and DGDG found in wheat flour.

2. Materials and methods

2.1. Purification of wheat galactolipids

In order to obtain highly pure galactolipids, devoid of residual pigments and traces of silica, a new purification procedure has been developed. These contaminants could impair the interface behavior and especially a good aqueous dispersion of the galactolipids as previously noted [17]. 500 g of a commercial wheat (*Triticum aestivum*) flour was stirred for 2 h with 1.5 L of dichloromethane–methanol (2:1 v/v). The slurry was filtered through a Buchner funnel and re-extracted with 1.5 L of the dichloromethane–methanol mixture. After evaporation of the solvent, the crude lipid extract was washed by phase partitioning in dichloromethane–methanol–aqueous NaCl 0.9% (8:4:3 v/v) to eliminate non-lipid substances [18]. The lower dichloromethane-rich phase was recovered and the solvent evaporated. The crude wheat flour lipid extract was fractionated by adsorption chromatography on silicic acid (Fluka, Buchs, Switzerland). Non-polar lipids, MGDG and DGDG enriched fractions were eluted with dichloromethane, dichloromethane–acetone (1:1 v/v) and acetone, respectively. Pure DGDG and MGDG were purified at 20 °C from the corresponding galactolipid fractions by normal phase high performance liquid chromatography (HPLC) on a column (10 mm × 250 mm) packed with Nucleosil Si 100, 5 μm pore size. The mobile phase was acetone–dichloromethane (70:30 v/v) and acetone–chloroform (1:1 v/v) for the DGDG and MGDG fractions, respectively. The injection volume was 1 mL containing about 30 mg crude lipids and the flow rate was 3 mL/min. Galactolipids were detected by differential refractometry (RID model 133, Gilson, France). Purity of DGDG and MGDG was controlled by thin layer chromatography on silica gel plates using chloroform–methanol–25% ammonia (13:7:1 v/v) for migration. Lipids were revealed under UV light after spraying with an ethanolic solution of rhodamine B. After evaporation of the solvent under vacuum, pure DGDG and MGDG were thoroughly dried under a nitrogen stream, weighed and finally solubilized in $CHCl_3$. Concentration of the DGDG and MGDG chloroform solutions were 45.9 mg/mL and 34.7 mg/mL, respectively. Analysis of galactolipid molecular species was carried out by reverse-phase HPLC on a column (7.5 mm × 250 mm) packed with Nucleosil C18 Si 100 5 μm pore size, with a UV detector at 210 nm. The mobile phase was methanol–water–acetonitrile (90.5:7:2.5 v/v/v) at 20 °C and at a flow rate of 0.5 mL/min [19]. Four major species were highlighted for MGDG corresponding to C18:2 $^{\Delta 9,12}$/C18:3 $^{\Delta 9,12,15}$ (11%), C18:2 $^{\Delta 9,12}$/C18:2 $^{\Delta 9,12}$ (75%), C16:0/C18:2 $^{\Delta 9,12}$ (5%) and C18:2 $^{\Delta 9,12}$/C18:1 $^{\Delta 9}$ (9%). The proportion of the different species is expressed in % of total absorbance at 210 nm. Similar molecular species were observed for DGDG, i.e., C18:2 $^{\Delta 9,12}$/C18:3 $^{\Delta 9,12,15}$ (12%), C18:2 $^{\Delta 9,12}$/C18:2 $^{\Delta 9,12}$ (65%), C16:0/C18:2 $^{\Delta 9,12}$ (20%) and C18:2 $^{\Delta 9,12}$/C18:1 $^{\Delta 9}$ (3%) [20]. The fatty acid composition of DGDG and MGDG was determined by gas-chromatography on a HP-5890 gas chromatograph equipped with a DB5 capillary column (Agilent Technologies, CA, USA) (30 m × 0.32 mm, film thickness 0.25 μm) of the corresponding methyl esters obtained by transesterification of the galactolipids in 14% boron fluoride in methanol. The fatty acid composition permitted the estimation of the mean molecular masses of MGDG and DGDG, i.e., 777 and 935 g/mol, respectively. The chemical structures of MGDG and DGDG are presented in Fig. 1.

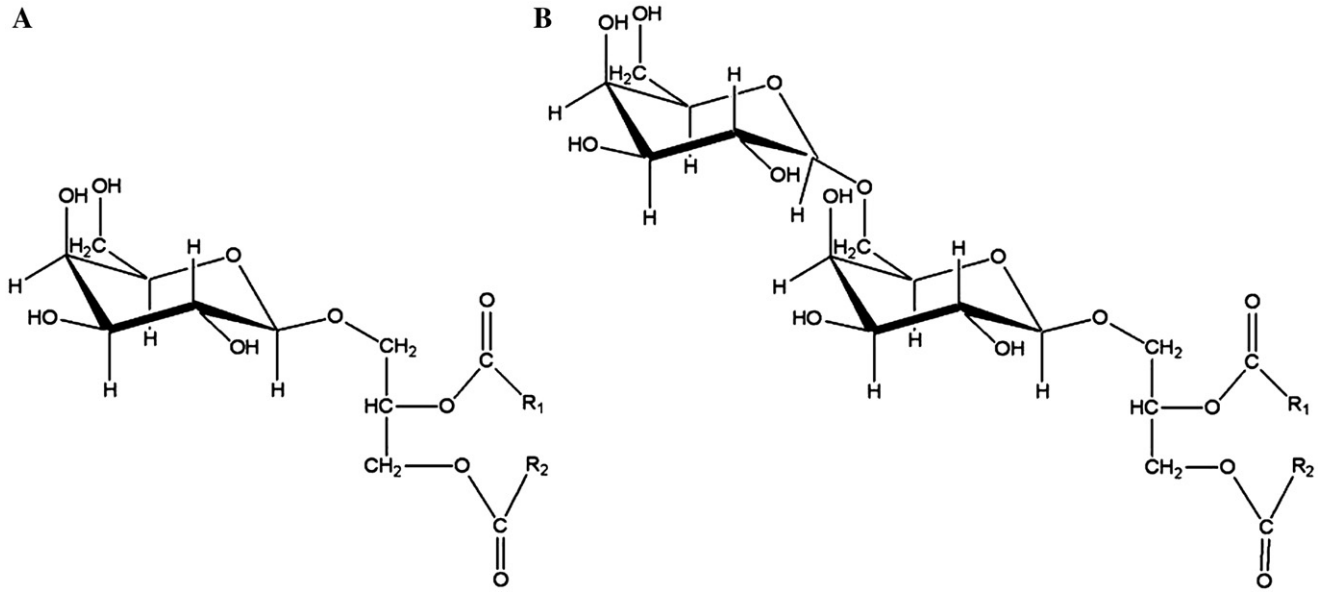

Fig. 1. Chemical structures of the natural wheat galactolipids studied here. A: MGDG and B: DGDG. The composition of the acyl chains R_1 and R_2 (number of carbon atoms and insaturations) is given in the purification part in Materials and methods.

2.2. Pressure–area isotherms

A computer-controlled and user-programmable Langmuir trough of 700 cm^2 (Nima Technology, Cambridge, UK) equipped with two movable barriers was used for the pressure–area isotherm recording. The surface pressure was measured with a filter paper held by a Wilhelmy balance connected to a microelectronic feedback system ($\pi = \gamma_0 - \gamma$, where γ_0 and γ are the surface tension values in the absence and presence of lipids at the air/liquid interface, respectively). Before starting the experiment, the trough was cleaned with chloroform and Millipore water. It was then filled up with 425 mL of the subphase (NaCl 0.1 M) and the air/liquid interface was cleaned of impurities by repeated aspiration and verification of the (π–A) isotherm each time. A good baseline in the π–A isotherms indicated the cleanliness of the interface. The galactolipids ($C = 10^{-3}$ M) in chloroform/methanol (2:1) were spread at the air/liquid interface using a high precision Hamilton microsyringe. After evaporation of the solvent (10 min), the π–A isotherm of lipid monolayer was measured by compressing the barriers at the rate of 20 cm^2/min. The temperature was kept constant at 19.0 ± 0.5 °C. Each experiment was repeated at least three times.

2.3. Ellipsometry

Ellipsometry was performed with a home-made ellipsometer [21] using a He–Ne laser ($\lambda = 632.8$ nm, Melles Griot, Carlsbad, CA) polarized with the aid of a Glan–Thompson polarizer (Melles Griot). The incidence angle of the light on the surface was 1° away from the Brewster angle. After reflection on the water surface, the laser light was passed through a $\lambda/4$ retardation plate, a Glan–Thompson analyzer and detected using a photomultiplier tube. Through a computer controlled feedback loop, the analyzer automatically rotated toward the extinction position. In this 'null ellipsometer' configuration [22], the analyzer angle, multiplied by 2, yielded the value of the ellipsometric angle (Δ), i.e., the phase difference between parallel and perpendicular polarizations of the reflected light. The laser beam probed a surface of 1 mm^2 and a depth of the order of 1 μm. The surface tension was measured with a filter paper held by a Wilhelmy balance. Initial values Δ_0 and γ_0 of the ellipsometric angle and surface tension were recorded on the subphase for 10 min. Ellipsometry measurements were performed at 19.0 ± 0.5 °C on a 7 × 10 cm^2, 60 ml rectangular Teflon Langmuir trough with a computer-controlled barrier (Nima Technology, Cambridge, UK). As mentioned above, lipids were spread at the air/water interface in a chloroform–methanol solution until the surface pressure became measurable (> 0.1 mN/m) and were then equilibrated for 10 min to allow the evaporation of the solvent. The lipid monolayers were compressed at the rate of 2 cm^2/min and values of Δ and π were recorded every 2 s with a precision of ±0.2° and ±0.1 mN/m, respectively.

2.4. Polarization modulation-infrared reflection absorption spectroscopy

The PM-IRRAS spectra of galactolipid monolayers at the air/liquid interface were recorded at 19.0 ± 0.5 °C on a Nicolet (Thermo Electron, Madison, WI) 870 FT-IR spectrometer with a spectral resolution of 8 cm^{-1} by co-adding 600 scans (corresponding to an acquisition time of 10 min). The film surface pressure was maintained at 35 mN/m during the measurement. The details of the optical setup, the experimental procedure and the two-channel processing of the detected intensity have been already described [23]. The interpretation of PM-IRRAS spectra in terms of molecular orientation relies on a specific surface selection rule which connects the intensity and the sense of the bands (i.e., positive or negative) to the orientation, relative to the interface, of the transition moment [24].

2.5. Atomic force microscopy

AFM imaging of Langmuir–Blodgett films (LB films) was performed in contact mode using a Pico-plus atomic force microscope (Molecular Imaging, Phoenix, AZ) under ambient conditions, using a 10 × 10 μm^2 scanner. Topographic images were acquired in constant force mode using silicon nitride tips on integral cantilevers with a nominal spring constant of 0.06 N/m. Images were obtained from at least two different samples prepared on different days with at least five macroscopically separated areas on each sample. Samples were made by transferring the LB film to freshly cleaved mica plates. To that end, the galactolipid monolayers were prepared as explained in the pressure–area isotherms above and compressed at 15 and 35 mN/m. All lipid layers were deposited at a constant surface pressure by raising vertically (1 mm/min) freshly cleaved mica through the air/liquid interface.

2.6. X-ray scattering

For the X-ray scattering experiments, lipid samples (1 mg of lipids hydrated with 200 μL of water) were deposited in glass capillaries of calibrated diameter ($1.4 < \varnothing < 1.5$ mm, Muller, Berlin, Germany) sealed with paraffin. Small-angle X-ray scattering was performed on the high brilliance ID2A beamline of the European Synchrotron Radiation Facility (ESRF, Grenoble, France) and at

station D43 beamline of Laboratoire pour l'Utilisation du Rayonnement Electromagnétique (LURE, Orsay, France). On ID2A [25], the sample-detector distance applied for the SAXS experiments, was 1.4 m. The X-ray patterns were detected and recorded via a CCD (chip charge-coupled device) camera detector between $q=0.02$ to 0.5 $Å^{-1}$. On the D43 beamline, a monochromatic (1.45 Å) focused X-ray beam selected by a parabolic Ge (111) crystal was used. The beam was defined by a 500-mm collimator. The X-ray diffraction patterns were recorded, at exposure time of 30–50 min, using an image plate (15×20 cm^2) which was further digitized for analysis [26]. In the same setup, two sample-to-detector distances (140 and 268 mm) were used to determine either the supramolecular organization of the lipid/water systems (SAXS) or the chain fluidity (WAXS). On both beamlines, the same sample holder was used. It could accommodate up to seven samples simultaneously and was thermostated by a computer-controlled oven at 20±0.5 °C [27]. The diffraction spacing was calibrated using the lamellar peaks of silver behenate ($d=58.380$ Å) as standard [28,29]. All samples exhibited powder diffraction profiles and the scattering intensities were determined by circular integration as a function of the radial wave vector, i.e., $q=(4\pi/\lambda)\times\sin(\theta)$ [30].

2.7. Raman spectroscopy

The Raman spectra of galactolipid dispersions in D_2O contained in melting point glass capillaries (5% w/v) were recorded at 20.5±0.5 °C in the back-scattering configuration using a LabRam 800HR Raman spectrometer (Jobin Yvon Horiba, Villeneuve d'Ascq, France) coupled to an Olympus BX 30 fixed stage microscope. The 514.5 nm line of an argon ion laser (Coherent, 70C Series Ion Laser, Santa Clara, CA) was focused with a 10× objective (0.25 NA-Olympus) generating an intensity of approximately 20 mW at the sample. The confocal hole and the entrance slit of the monochromator were fixed at 300 and 100 μm, respectively. By using 600 lines/mm holographic grating, spectral windows of approximately 2000 cm^{-1} were collected for each exposure by the 1-in. open electrode Peltier-cooled CCD detector (1024×256 pixels) (Andor Technologies, Belfast, Northern Ireland). The spectra were obtained from 40 acquisitions with an integration time of 20 s each. All spectral manipulations were performed using GRAMS/AI 7.0 (ThermoGalactic, Salem, NH). The spectra were 5 or 9 points smoothed and corrected for a slight fluorescence background using a polynomial baseline.

2.8. Fourier transform infrared spectroscopy

The attenuated total reflectance (ATR) spectra were recorded at 20.5±0.5 °C using a Magna 760 Fourier transform infrared spectrometer (Thermo-Electron, Madison, WI) equipped with an MCT detector (mercury–cadmium–telluride detector). A motorized rotating ZnSe wire-grid polarizer (Specac, Orpington, UK) was positioned in front of the sample to obtain parallel (p) and perpendicular (s)-polarized spectra without breaking the purge of the spectrometer. The germanium ATR crystal (50×20×2 mm, 45° parallelogram) was placed in a home-made horizontal ATR accessory. An amount of 0.5 mg of lipids in chloroform/methanol was deposited on the ATR crystal. After solvent evaporation (10 min), lipids were hydrated with 20 μL ultrapure water (Millipore). A metallic cell was put on the top of the sample to avoid water evaporation due to the purge of the spectrometer. A total of 400 scans with a resolution of 4 cm^{-1} was sufficient to achieve a high signal-to-noise ratio. The position of the band maxima was determined from the middle of the pick at 90% of their height [31].

3. Results

3.1. Galactolipid monolayers at air/liquid interfaces

Investigating the properties of galactolipid Langmuir films formed at the air/liquid interface involved coupling of different techniques which provide information on the area occupied by the molecules at the maximum point of compressibility (pressure–area isotherms), monolayer thickness (ellipsometry), orientation and hydration of the polar headgroups (PM-IRRAS) and on the overall organization of the monolayers at low (15 mN/m) and high (35 mN/m) surface pressures (AFM).

3.2. Pressure–area isotherms

Fig. 2 shows the (π–A) isotherms of MGDG, DGDG and MGDG/DGDG (1/1 molar ratio) monolayers spread on the subphase at 19.0±0.5 °C. All pressure–area isotherms display a regular increase, with neither shoulder nor inflexion point, of the surface pressure until the collapse is reached. This indicates the presence of a single, homogeneous liquid-expanded (LE) phase in agreement with the high degree of double bonds in the acyl chains that limits molecular packing [32]. This expanded monolayer behavior was described in a study of chloroplast lipids where the insaturation number was controlled [33] or in phospholipid monolayers [34]. The collapse pressures are close to 46 mN/m for MGDG and DGDG, and 47 mN/m for mixed monolayer as observed previously for the corresponding galactolipids of barley leaves [35]. These high values indicate a good purity of lipids as emphasized by Tancrede et al. [36]. As shown in Fig. 2, DGDG occupies a lower mean molecular area than MGDG or the equimolar mixture at all surface pressures. The minimal mean molecular area determined at the intercept between the tangent to the collapse plateau and the tangent to the end of the pressure–area isotherm is 64 $Å^2$/molecule for DGDG, 82 $Å^2$/molecule for MGDG and 70 $Å^2$/molecule for the equimolar mixture. Although DGDG possesses two galactosyl headgroups and MGDG only one, its minimal area at the interface is smaller than that of MGDG, as previously observed by Gallant and Leblanc [35]. Two factors could usually affect the minimal mean molecular area, the presence of double bonds on the acyl chains and the interactions between headgroups. There are significant differences between the acyl chain compositions of MGDG and DGDG and especially concerning the saturated fatty acid C16:0. DGDG contains 10% of C16:0 against 2.5% for MGDG. Thus, the lower mean molecular area of DGDG could be in part attributed to this variation. Nevertheless, the effect of

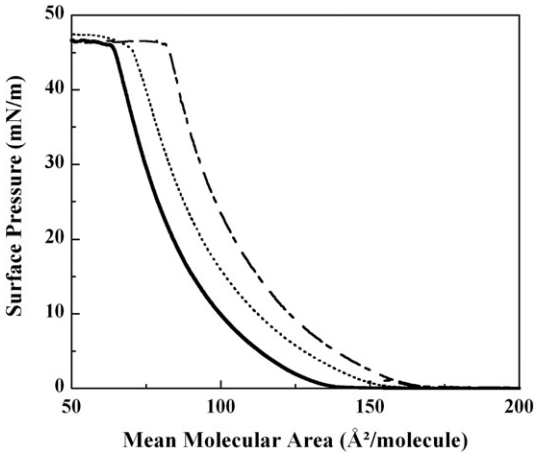

Fig. 2. (π–A) isotherms of the galactolipids. DGDG (solid line), MGDG (dashed-dotted line) and equimolar mixture (dotted line) monolayers at the air/liquid interface. The constant temperature was 19.0±0.5 °C.

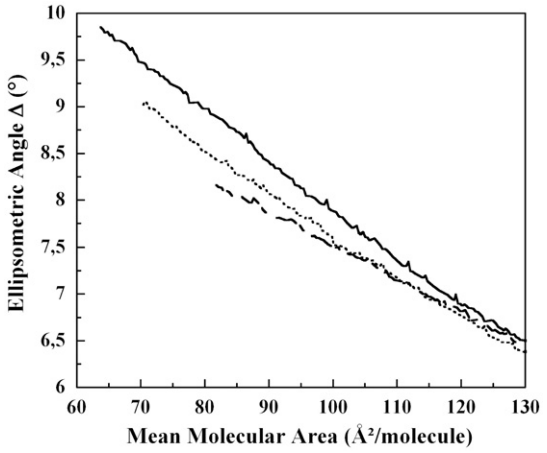

Fig. 3. (Δ–A) curves of the galactolipids. DGDG (solid line), MGDG (dashed-dotted line), and equimolar mixture (dotted line) monolayers at the air/liquid interface performed at 19.0±0.5 °C.

the galactosyl headgroups, in particular the orientation of these, cannot be excluded. First, because the saturated chain C16:0 is always associated with an unsaturated one. Furthermore, the increase of the number of sugar residues in the polar headgroup of glycolipids does not lead necessarily to an increase of the molecular area, and can even sometimes result in a decrease of the molecular area, as observed by Tamada et al. [37].

3.3. Ellipsometry

Fig. 3 shows the effect of the molecular area on the ellipsometric angle (Δ) for the monolayers formed by MGDG, DGDG and their equimolar mixture. The standard deviation for ellipsometric data is ±0.07° for DGDG, ±0.04° for MGDG and ±0.14° for mixed film. Each monolayer was compressed until the collapse pressure where structures appeared that are no longer representative of a monolayer behavior. At the initial molecular area, the ellipsometric angle Δ is nearly the same for all galactolipid monolayers. Below 120 Å^2/molecule, the ellipsometric angle Δ becomes higher for DGDG than for MGDG and as for the pressure–area isotherms, no plateau is observed. The final ellipsometric angles are 9.85° for DGDG, 9.04° for the mixture and 8.10° for MGDG. At the point of maximal compressibility, i.e., beginning of the collapse, the difference is at least 1.64° between MGDG and DGDG ellipsometric angles. According to De Feijter et al. [38], Δ is sensitive to variations of the refractive index and the thickness of the monolayer. Considering that there is a majority of C18:2 in the mixtures of acyl chains of MGDG and DGDG, the refractive indices and the thicknesses of the fluid hydrophobic parts should be extremely close. Thus, the ellipsometric angles should vary similarly during the compression as observed by Ducharme et al. [39]. Nevertheless, the slopes between the curves of both MGDG and DGDG are clearly different (Fig. 3). This demonstrates the necessity to consider the contribution of headgroups, as indicated by Tamada et al. [37]. In our case, the differences observed for MGDG and DGDG should be attributed either to different refractive index or to different thickness of the polar parts. The nature of the headgroups is identical (galactosyl) and the variation of refractive index between one and two galactosyl groups cannot justify the great difference observed between MGDG and DGDG (1.64° for the collapse pressure). Moreover, at high mean molecular area (130 Å^2/molecule) the ellipsometric angles are similar for both galactolipids. Therefore, the variations of Δ should be essentially affected by the variations of the thickness of the film. According to these results, the thickness of the DGDG film should be greater than that of the MGDG film, whereas an intermediate thickness is displayed for the mixture.

3.4. PM-IRRAS

Fig. 4 shows the PM-IRRAS spectra in the 1850–950 cm^{-1} spectral range of the galactolipid monolayers compressed at 35 mN/m. The main vibrational modes of the polar headgroups are observed in this spectral range, i.e., the stretching vibration of carbonyl group (νC═O, around 1735 cm^{-1}), the IRRAS specific effect of water (around 1665 cm^{-1}), and the stretching vibration of the C–O–C bonds of the galactosyl groups (around 1050 cm^{-1}). The spectra show some differences for the sharp band assigned to the C═O stretching vibration. Actually, a shift to lower wavenumbers is detected between MGDG (1736 cm^{-1}), DGDG (1734 cm^{-1}) and the equimolar mixture (1729 cm^{-1}). The broad dip located around 1665 cm^{-1} present in the MGDG and DGDG spectra is an optical effect specific to the IRRAS technique and is due to the strong dispersion of the refractive index of liquid water in the spectral range of the bending mode. For the equimolar mixture, the spectrum in this region is markedly different from those of the pure lipids with disappearance of the dip and the appearance of a positive band at 1670 cm^{-1} and of a negative one at 1545 cm^{-1}. This phenomenon means that the interfacial water molecules are strongly perturbed in the case of the equimolar mixture. The band at 1464 cm^{-1} is assigned to the bending mode of the methylene of the acyl chains of the lipids. Finally, significant

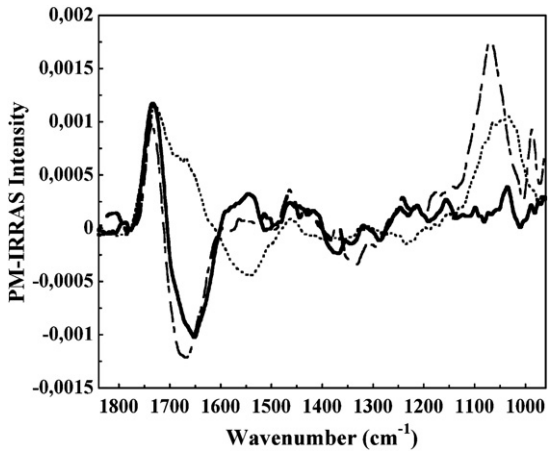

Fig. 4. PM-IRRAS spectra of the galactolipids in the 1850–950 cm^{-1} spectral range. DGDG (solid line), MGDG (dashed-dotted line) and equimolar mixture (dotted line). The monolayers at the air/liquid interface were compressed at 35 mN/m and the temperature was maintained at 19±0.5 °C.

changes are also observed in the 1100–1000 cm^{-1} range corresponding to the stretching vibration of the C–O–C bonds of the galactosyl groups. For the MGDG monolayer, a positive band centered at 1068 cm^{-1} is observed that is absent for the DGDG one, although a very small contribution appears at 1035 cm^{-1}. For the equimolar mixture, a broader and less intense band appears at 1045 cm^{-1} that could apparently be decomposed in two bands centered at 1068 cm^{-1}, as observed for MGDG alone, and at 1035 cm^{-1} with equivalent intensity.

Applying the selection rules at the air/liquid interface established by Blaudez et al. [24], we have determined the orientation of the galactosyl headgroups. Actually, the positive C–O–C band for MGDG corresponds to a parallel orientation of the mono-galactosyl groups with respect to the interface whereas the absence of this C–O–C band for DGDG is characteristic of an average tilt angle of 40° of the di-galactosyl groups with respect to the normal to the interface. For the equimolar mixture, the band at 1035 cm^{-1} could be due to the digalactosyl headgroups of DGDG while the band at 1068 cm^{-1} could be due to MGDG. This hypothesis is supported by the fact that the intensity of the MGDG band in the mixture is two times lower due to the dilution effect in the galactolipid equimolar mixture. This suggests that, in the mixture, the monogalactosyl headgroup of MGDG forces the digalactosyl group to adopt an orientation that is more parallel to the interface.

3.5. Atomic force microscopy

The LB films of pure MGDG, DGDG and equimolar mixture were examined by AFM at 15 and 35 mN/m (Fig. 5). All films are homogeneous at 15 mN/m with no visible phase separation or segregation. No change is observed for DGDG LB films when increasing the surface pressure up to 35 mN/m, while a segregation is observed for MGDG and the equimolar mixture. As seen in Fig. 6, these segregated structures are better resolved when a small area is scanned. In the case of MGDG, interconnected protrusions cover the surface, whereas small isolated patches are observed for the mixed film. Also, the horizontal cross-sections (Fig. 6) have permitted the estimation of the height of the observed structures which are close to 7 Å for MGDG and 4 Å for the mixture. The shape of MGDG structures was irregular, whereas mixed films formed round domains with a diameter of approximately 100 nm.

3.6. Galactolipid liquid-crystalline mesophases

The phase behavior, i.e., the liquid-crystalline organization of galactolipid dispersions in water, was investigated by small-angle X-ray scattering. In the case of the pure MGDG and DGDG, the electron density was reconstructed giving crucial information on the molecular packing of the galactosyl head-

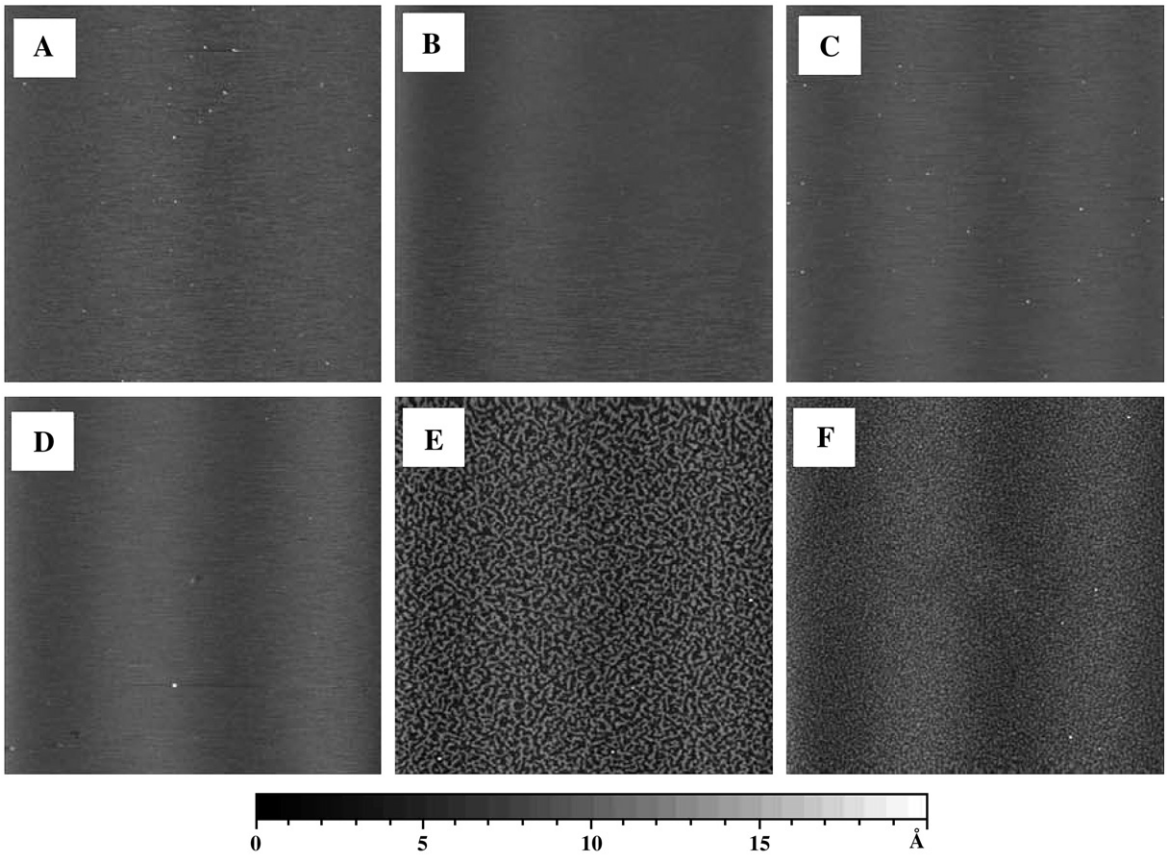

Fig. 5. AFM topographic images of the galactolipid LB films transferred at low and high surface pressures. A, B, C: DGDG, MGDG, and equimolar mixture respectively at π=15 N/m. D, E, F: DGDG, MGDG and equimolar mixture respectively at π=35 mN/m. The scan size is 8 μm×8 μm. Gray scale: *z*-range is 20 Å meaning that higher objects appear lighter.

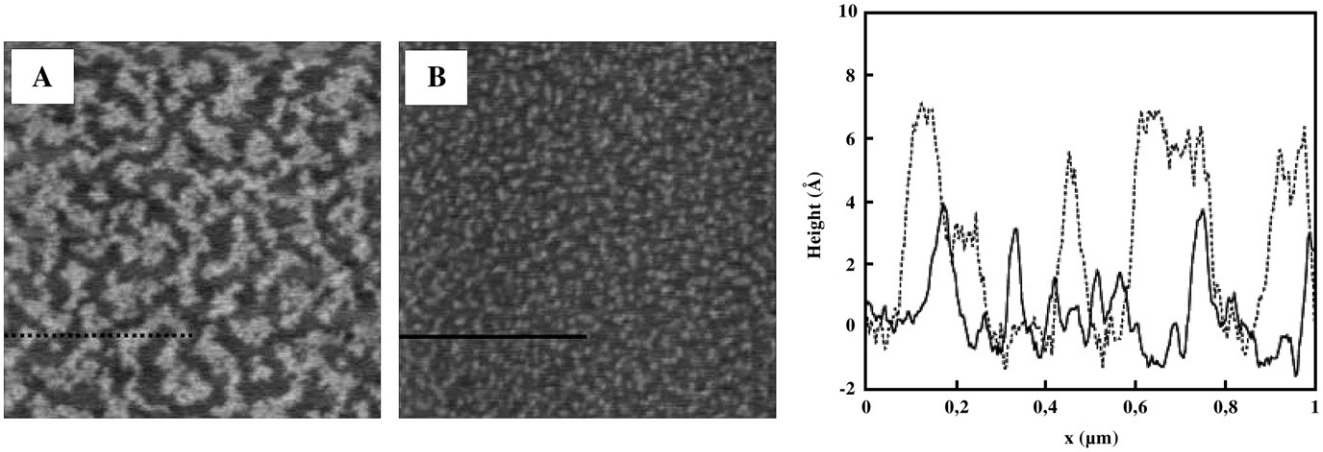

Fig. 6. AFM topographic images of LB films transferred at 35 mN/m. A, B: MGDG and equimolar mixture, respectively. The scan size is 2 µm × 2 µm. Horizontal cross-sections show the height difference between the protrusions of the MGDG and the equimolar mixture. Gray scale: *z*-range is 20 Å.

groups. Complementary measurements by vibrational spectroscopies (Raman and FT-IR) provided information on the orientation of the acyl chains.

3.7. X-ray scattering

The three-dimensional structures of MGDG, DGDG and their equimolar mixture in excess water were determined by analysis of the X-ray diffraction patterns at 20 °C. Two regions were used to identify the lipid phases. The small-angle region provides structural information on the phase symmetry and long-range organization (cubic, hexagonal or lamellar phases), whereas the wide-angle region provides information on the hydrocarbon chain packing (fluid or gel phases). For all samples, the presence of a diffuse signal in the wide-angle region (for $q \sim 1.4$ Å^{-1}, data not shown) indicates that the hydrocarbon chains are undergoing rapid motion typical of fluid phase.

3.8. Lamellar phase of the DGDG/water system

Fig. 7A shows the small-angle X-ray diffraction profile obtained for the DGDG dispersion. The presence of single peaks regularly spaced reveals a lamellar structure L_α. The observed positions (q_{obs}) of the four Bragg reflections and the theoretical positions ($q_n = 2\pi n/d_{lam}$) calculated with a lamellar periodicity (d_{lam}) of 54.85 Å are given in Table 1. The lamellar spacing of 54.9 Å is consistent with that obtained by Shipley et al. [40] for DGDG purified from *Pelargonium* leaves (54.0 Å) and by Sen et al. [41] for DGDG extracted from bean leaves (55.3 Å). To obtain more molecular information on the headgroup conformation, the electron density perpendicular to the bilayer surface was reconstructed.

The electron density profile was calculated from measured intensities of the reflections in diffraction pattern and using the phase combination [26,42]. The electron density variations are related to the Bragg peak intensities by

$$\Delta\rho(x) = \sum_n F_n^{obs} \times \cos(2\pi n x), \quad (1)$$

with, after Lorentz polarization corrections at small angles,

$$|F_n^{obs}| = q_n \times \sqrt{A_n}, \quad (2)$$

where F_n^{obs} is the structure factor, q_n the positions of the Bragg reflections and A_n the area of the Bragg reflection.

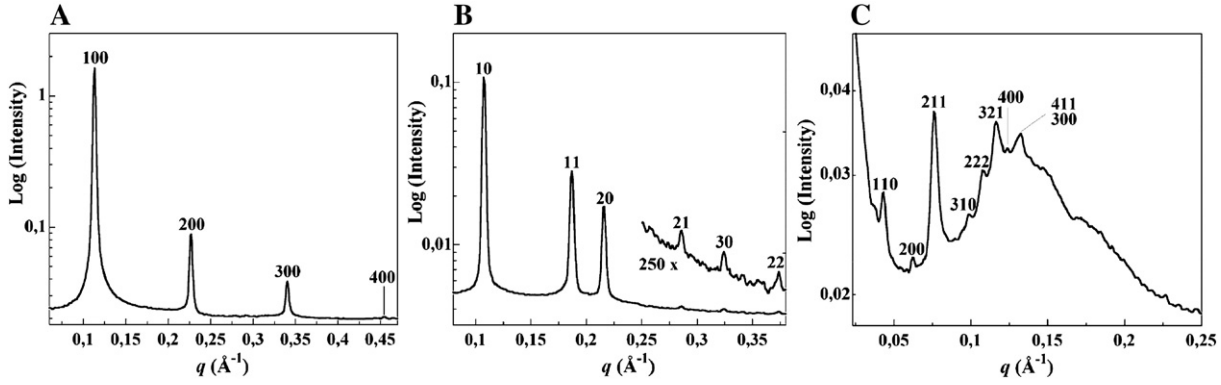

Fig. 7. SAXS patterns of the galactolipid/water systems recorded at 20±0.5 °C. A: DGDG/water system, the indexation (*h*00) is also shown. B: MGDG/water system, the indexation (*hk*) is also shown. From $q = 0.25$ Å^{-1}, the trace is scale-expended to make visible the higher order of Bragg peaks. C: equimolar mixture/water system, the indexation (*hkl*) is also shown.

Table 1
SAXS data of the lamellar phase of the DGDG/water system at 20 °C

h 0 0	n [a]	q_{obs}(Å^{-1}) [b]	q_n(Å^{-1}) [b]	F_{obs} [c]
1 0 0	1	0.1144	0.1145	−100
2 0 0	2	0.2289	0.2291	−42
3 0 0	3	0.3436	0.3436	−36
4 0 0	4	0.4584	0.4582	+11

[a] n is the Bragg reflection order.
[b] q_{obs} and q_n are respectively the observed and calculated ($q_n=2\pi n/d_{lam}$, with the lamellar periodicity d_{lam} equal to 54.85 Å) positions of the (h00) small-angle reflections.
[c] F_{obs} is the structure factor calculated from Eq. (2) and normalized using the value of the first peak; the chosen phase of F_{obs} (+ or −) is deduced from the criteria described in the text.

Due to the centrosymmetry of the lamellar structure, the phase of F_n^{obs}, is restricted to be either 0 or π, and consequently $F_n^{obs} = \pm qn \times \sqrt{A_n}$.

As a result, to determine the electron density profile, the sign of each F_n^{obs} has to be determined. It is worthy to note that the $x=x+d_{lam}/2$ translated solution only changes the sign of the F_n^{obs} for even n because:

$$\Delta\rho\left(x+\frac{d_{lam}}{2}\right)=\sum_n F_n^{obs}\times(-1)^n\cos(2\pi nx) \quad (3)$$

Therefore, observation of n Bragg reflections gives 2^n available electron density variations. As there is an identical translated solution in the case of each electron density, there are only 2^{n-1} non-equivalent solutions.

Four peaks were observed on the diffraction profile of DGDG leading to 8 possible solutions. Simple molecular assumptions on the electron density profile in the bilayer [43] allowed us to exclude false solutions. These criteria were: (1) the galactosyl headgroup must have the highest electron density, (2) the electron density must be constant along the acyl chain, and (3) the minimum corresponding to the terminal methyl must be narrow. F_{obs} values with the corresponding sign are listed in Table 1 for the only solution respecting these three criteria, and the corresponding electron density is shown in Fig. 8. The first minimum ($x=0$ Å) corresponds to the terminal methyl group. The electron density is constant along the hydrocarbon chain up to a maximum attributed to the polar headgroup ($x=18.8$ Å). After this point, the electron density decreases up to a minimum ($x=27.5$ Å) attributed to the center of the water layer; then, the profile becomes symmetric. This profile looks like that described by McDaniel for DGDG extracted from *Briza humilis* seeds using neutron diffraction [44]. In accordance with this profile, the length of the acyl chains is estimated to be 15 Å meaning that the thickness of the hydrophobic core is 30 Å. Furthermore, a headgroup length of about 18 Å was estimated for a DGDG molecule using the CPK atomic model taking into account the two linked galactosyl rings and the glycerol part. According to the density profile, the thickness of a headgroup is estimated to be 8 Å. Thus, it is clear that the headgroups are not completely extended but oriented parallel to the plane of the bilayers, as indicated in Fig. 8.

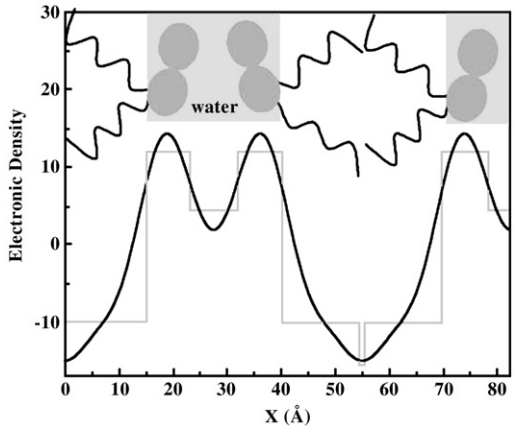

Fig. 8. Electron density profile calculated for the lamellar fluid phase (L_α) formed by the DGDG/water system and the corresponding single three-step model. A schematic view of the organization of three DGDG molecules highlighting the orientation of sugar headgroups is associated to this profile.

3.9. Hexagonal phase of the MGDG/water system

Fig. 7B shows the X-ray diffraction profile obtained for MGDG. The six detected peaks of the Bragg diffraction could be indexed with ratios of 1, $\sqrt{3}$, $\sqrt{4}$..., that is, a characteristic of a hexagonal phase called H. The observed positions (q_{obs}) of the (hk) reflections, the theoretical positions ($q_n=4\pi\sqrt{n}/\sqrt{3}d_{hex}$, with $n=h^2+hk+k^2$) calculated with an hexagonal periodicity (d_{hex}) of 67.2 Å and the structural factor (F_{obs}) with its sign are listed in Table 2. Two kinds of hexagonal structures are generally described. The direct hexagonal H_I structures are lipid rods, where acyl chains form the hydrophobic core, stacked up to form a hexagonal pattern. On the contrary, the inverse hexagonal phase H_{II} is characterized by hexagonal stacking of water cylinders covered by polar headgroups and acyl chains directed outside. Usually the hexagonal phase H_I should not exist in the presence of excess water. Actually, as water is added in the system, the H_I structure swells up to be in equilibrium with micellar structures.

In our case, neither the lattice parameter variation nor the presence of micelles was detected whatever beam position.

Table 2
SAXS data of the hexagonal phase of the MGDG/water system at 20 °C

h k	n [a]	q_{obs}(Å^{-1}) [b]	q_n(Å^{-1}) [b]	F_{obs} [c]
1 0	1	0.1077	0.1080	+100
1 1	3	0.1870	0.1870	+87
2 0	4	0.2159	0.2159	−74
2 1	7	0.2857	0.2856	+11
3 0	9	0.3243	0.3239	−13
2 2	12	0.3733	0.3740	+13

[a] $n=h^2+hk+k_2$.
[b] q_{obs} and q_n are respectively the observed and calculated ($q_n=4\pi\sqrt{n/\sqrt{3}d_{hex}}$, with the hexagonal periodicity d_{hex} equal to 67.2 Å,) positions of the (hk) small-angle reflections.
[c] F_{obs} is the structure factor calculated from Eq. (2) and normalized using the value of the first peak; the chosen phase of F_{obs} (+ or −) is deduced from the criteria described in the text.

Therefore, the structure of hydrated MGDG mesophase corresponds to the inverse hexagonal phase H_{II}. This result is in good agreement with previous data [40]. From the d_{hex} parameter, and taking into account the headgroup size of 9 Å (CPK atomic model: one galactosyl ring and the glycerol part) and the chain length of 18 Å (octadecane chain in fluid phase), the estimated diameter of the water channel should be rather important, i.e., around 13.2 Å. To obtain more precise information on the molecular organization the electron density was reconstructed.

The radial electron density was reconstructed perpendicularly to the water channel applying the following formula [45] on the observed diffraction peaks:

$$\rho_{el}(r) \propto \sum_{n=1,3,4,7,9,12} F_n \times J_0 \times \left(2\pi r 2 \times \sqrt{\frac{n}{\sqrt{3}\times d}}\right) \quad (4)$$

where, F_n is the structural factor of the q_n peaks, J_0 is the 0 order of the Bessel function, r is the distance from the center of the water channel, d is the lattice parameter of the hexagonal structure, and n is equal to h^2+hk+k^2.

As in the case of the lamellar phase, the electron density is reconstructed using a specific choice of phase combinations. With 6 peaks in the diffraction pattern, 2^6 such solutions exist. To eliminate false solutions, some criteria were used. Considering the fact that the electron density of the sugar headgroup is higher than that of the water and since the value for the water is higher than that of the corresponding acyl chains, three levels appear. The origin of the graph is the center of the water channel (intermediate density). Then, the electron density presents a maximum (headgroup) followed by a significant and slow decrease along the acyl chains up to the methyl group. Fig. 9 shows the only solution that satisfies these criteria. Considering a chain length of 18 Å (compared with DOPC chains in fluid phase) and a mono-galactosyl headgroup of 9 Å, and knowing the radius of the cylinder (33.6 Å), the center of mass of sugar headgroups should be located at 11.1 Å (point C_{theo}). Nevertheless, the electron density shows the gravity center of MGDG headgroups (point C_{exp}) at 9.3 Å. This should indicate the existence of a roughness due to the fact that the headgroups are not in the same level (Fig. 9). This roughness can be evaluated as: $2\times(C_{theo}-C_{exp})=3.6$ Å. Finally, the water core is smaller than previously assumed which suggests a poorly hydrated structure.

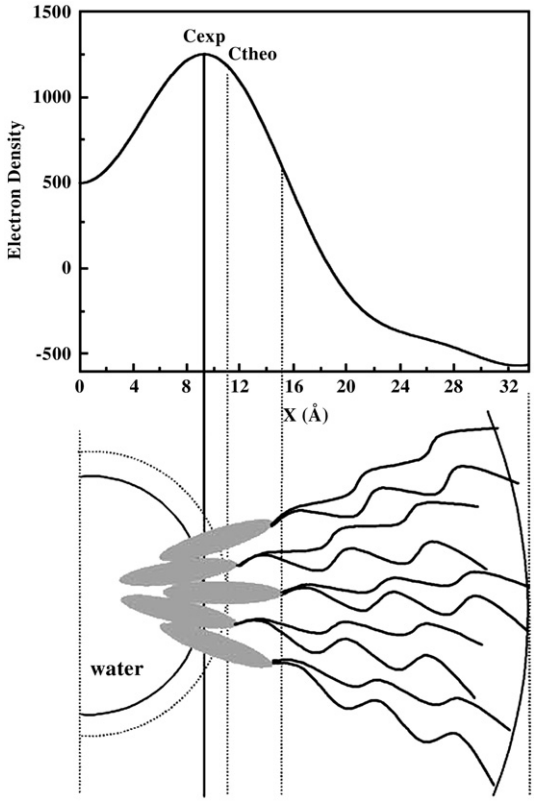

Fig. 9. Electron density profile calculated for the inverse hexagonal phase (H_{II}) formed by the MGDG/water system. A schematic view of the organization of five MGDG molecules highlighting the specific organization of sugar headgroups is associated to this profile.

3.10. Bicontinuous cubic phase of the MGDG/DGDG/water system

Fig. 7C shows a typical cubic diffraction profile obtained for an equimolar mixture of MGDG and DGDG in excess water. The observed positions (q_{obs}) of the (hkl) reflections and the theoretical positions ($q_n=2\pi\sqrt{n}/d_{cub}$, with $n=h^2+k^2+l^2$) calculated with a cubic cell parameter (d_{cub}) of 202 Å are listed in Table 3. At this stage, three space groups are possible: *Im3m*, *Ia3d* and *Pn3m*. Nevertheless, the observation of the (110) plane eliminates the *Ia3d* space group. As specified in Table 3, the systematic absence of odd ($h+k+l$) peaks supports the hypothesis of a centered lattice typical of the *Im3m* space group (Q^{229}). This phase should be described like an orthogonal network of water channels connected six-by-six and separated by lipid bilayers [46]. The cubic phase formation is usually expected to occur between lamellar and hexagonal phases for a pure single lipid component or mixed lipid hydrated systems [47]. Furthermore, a theoretical analysis has shown that the cubic phase has a smaller amount of frustration than these two phases [48]. It is generally difficult to obtain molecular information by reconstruction of the electron density but the existence of epitaxial relationships between specific planes of hexagonal and cubic phases is useful to extract molecular packing by similarity to related hexagonal phase [49]. The ratio between parameters of hexagonal and lamellar phases is $2/\sqrt{3}$ and between cubic and lamellar phases is $2/\sqrt{16}$ [50]. Then, between the hexagonal and cubic phase the quotient is equal to $1/2\sqrt{3}$. In our case, applying this rule, the diameter of the lipid cylinder surrounding the water channel should be 58.3 Å (d_{cub} /$2\sqrt{3}$). This diameter calculated for a DGDG/MGDG mixture in hexagonal phase is smaller than for the pure MGDG ($d_{hex}=67.2$ Å). This result is quite surprising because the addition of DGDG molecules with larger headgroups decreases the hexagonal lattice parameter. This result demonstrates a specific behavior of the equimolar mixture which is not directly related to the behavior to be expected from pure lipids.

Table 3
SAXS data of the cubic phase of the equimolar mixture/water system at 20 °C

h k l	n[a]	q_n (Å^{-1})[b]	q_{obs} (Å^{-1})[b]	Im3m[c]	Pn3m[c]
1 1 0	2	0.044	0.044	+	+
1 1 1	3	0.054	n.o	abs	+
2 0 0	4	0.062	0.062	+	+
2 1 1	6	0.076	0.076	+	+
2 2 0	8	0.088	n.o	+	+
3 0 0					
	9	0.093	n.o	abs	+
2 1 1					
3 1 0	10	0.098	0.099	+	+
3 1 1	11	0.103	n.o	abs	+
2 2 2	12	0.108	0.108	+	+
3 2 1	14	0.116	0.116	+	+
4 0 0	16	0.124	0.124	+	+
4 11					
	18	0.132	0.133	+	+
3 3 0					

n.o.=not observed.
[a] $n=h^2+k^2+l_2$.
[b] q_{obs} and q_n are respectively the observed and calculated ($q_n = 2\pi\sqrt{n/d_{cub}}$, with the cubic periodicity d_{cub} equal to 202 Å,) positions of the (*hkl*) small-angle reflections.
[c] These columns indicate which peaks are observed (+) or absent (abs) in each possible space group.

3.11. Raman and FTIR measurements

Fig. 10A shows the Raman spectra of the galactolipids in the 2000–2800 cm^{-1} range. The intensity of the broad peak observed in this region is due to the O–D stretching modes of D_2O. It reveals that the hydration of MGDG is quite low. On the contrary, the MGDG/DGDG equimolar mixture is highly hydrated. The bands due to the different C–H stretching vibrations of the acyl chains appear in the 2800–3050 cm^{-1} region (Fig. 10B). The symmetric and antisymmetric C–H stretching vibrations of methylene appear at 2856 and 2899 cm^{-1}, respectively. The shoulder at 2932 cm^{-1} is assigned to the Fermi resonance of the methyl symmetric stretching vibration while the peak around 2959 cm^{-1} is due to the asymmetric stretching vibration of this same group. Finally, the band due to the C–H stretching vibration of CH═CH bonds is observed at 3011 cm^{-1}. The positions of these bands (in wavenumbers) in the Raman spectra of MGDG and DGDG are compared in Table 4 to those obtained for DMPC and DOPC bilayers in an aqueous environment [51]. As can be seen in Fig. 10B, spectral differences are clearly observed for the equimolar mixture compared to the pure galactolipids. The band due to the methylene symmetric stretching vibration of the mixture is shifted to lower wavenumbers (2853 cm^{-1}) while the band due to the antisymmetric stretching vibration appears at higher wavenumbers (2905 cm^{-1}). It has been shown that the I_{2900}/I_{285O} intensity ratio (R_2) is a highly sensitive probe of the intermolecular vibrational coupling and consequently of the lateral packing of the acyl chains; it is also sensitive to the acyl chain dynamics [52,53]. On the other hand, the I_{2930}/I_{2900} ratio (R_1) provides a measure of the overall disorder of the lipid acyl chain matrix and in particular the conformational order [54,55]. The R_1 and R_2 ratios calculated for the three lipid systems are reported in Table 5. Both intensity ratios clearly show that the acyl chains are more ordered in the lipid mixture compared to

Table 4
Comparison of the wavenumber position of the C–H stretching vibrations observed by Raman spectroscopy of fully hydrated pure DMPC, POPC, MGDG, DGDG and equimolar mixture

	DMPC[a] (am^{-1})	POPC[a] (cm^{-1})	MGDG[a] (cm^{-1})	DGDG (cm^{-1})	(1:1) mixture (cm^{-1})
CH_2 symmetric stretching vibration	2851	2855	2856	2856	2856
CH_2 antisymmetric stretching vibration	2882	2893	2899	2899	2904
CH_3 symmetric stretching vibration	2928	2928	2932	2931	2931
CH_3 antisymmetric stretching vibration	2972	2972	2955	2960	2959

[a] [51].

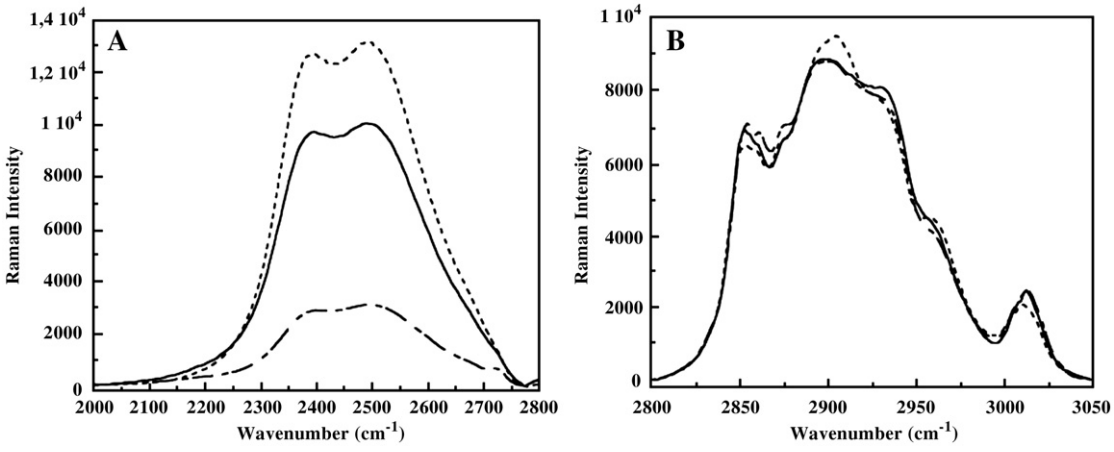

Fig. 10. Raman spectra of the galactolipid dispersions in D_20. DGDG (solid line), MGDG (dashed-dotted line), and equimolar mixture (dotted line). The spectra were normalized using the area under the band due to the C–H stretching vibrations between 2800 and 3050 cm^{-1} as an intensity standard. A: 2000–2800 cm^{-1} range characteristic of the O–D stretching modes of D_2O. B: 2800–3050 cm^{-1} range characteristic of the different C–H stretching vibrations of the acyl chains.

Table 5
Values of the intensity ratios $R_1 = I_{2930}/I_{2900}$ and $R_2 = I_{2900}/I_{2850}$ calculated from Raman spectra of MGDG, DGDG and equimolar mixture and corresponding values obtained from polarized ATR infrared spectra of the wavenumber position of the infrared band due to the antisymmetric CH stretching mode and of the order parameter S_z calculated for the symmetric CH stretching mode

	MGDG	DGDG	(1:1) mixture
$R_1 = I_{2930}/I_{2900}$	0.89	0.91	0.81
$R_2 = I_{2900}/I_{2850}$	1.26	1.36	1.47
ν_a (CH_2) (cm^{-1})	2925.7	2926.6	2925.4
S_z [ν_s (CH_2)]	−0.09	−0.09	−0.17

the pure lipids. Furthermore, as seen in Table 5, this finding is supported by the position of the band due to the antisymmetric C–H stretching vibration in the infrared spectrum (spectra not shown), which appears at lower wavenumbers for the equimolar mixture. Finally, the order parameter S_z of the transition moment [56] of the band due to symmetric C–H stretching vibration calculated from the polarized ATR spectra (data not shown) for hydrated MGDG, DGDG and equimolar mixture indicates a better alignment of the C–H bonds parallel to the ATR crystal for the equimolar galactolipid mixture.

4. Discussion

During the last step of seed development, a programmed dehydration process occurs that damages the integrity of the endosperm cell membranes. This apoptotic programmed end-event for the endosperm of wheat seeds leads to the accumulation of membrane remnants between the protein matrix and the starch granules. These remnants come from the membranes of protein bodies — vacuoles and amyloplasts [13]. In the dry seed, these membrane lipid remnants are organized in hexagonal, cubic and lamellar phases [13]. This phase behavior of membranes in dry wheat seeds is probably related to the phase behavior of their individual lipid components. MGDG and DGDG are the major lipids of amyloplast membranes and are also the major polar lipids of wheat endosperm. It is known that galactolipids purified from thylakoids form hexagonal (MGDG) and lamellar (DGDG) phases [40]. However, the novelty of this work lies in the fact that we have studied the phase behavior of galactolipids from amyloplast membranes and especially their binary mixture, which is close to that found in the natural system. While amyloplast galactolipids are rich in linoleic acid, i.e., C18:2, the galactolipids of thylakoid concentrate linolenic acid, i.e., C18:3. In order to highlight the influence of the aliphatic chains and of the mono- or di-galactosyl headgroups on the organization properties, our approach was to associate techniques dedicated to the study of the liquid-crystalline mesophases and others specifically investigating the nature of the self-assembly process in two dimensions.

For both MGDG and DGDG, the dilinoleyl lipid is the main molecular species (C18:2/C18:2). The presence of several double bonds in the acyl chains of polar lipids is known to prevent the formation of ordered phases as we observed with the wheat galactolipids. In fact, the results of the experiments performed on lipid monolayers at the air/liquid interface or in liquid-crystalline phase show a behavior typical of lipids in fluid phase. Surface–pressure isotherms of the monomolecular films are characteristic of liquid expanded phases with no shoulder or inflexion point (Fig. 2), whereas X-ray measurements in excess water show the presence of a diffuse signal in the wide-angle region. Additional information obtained from Raman and FTIR measurements confirms this behavior (Fig. 10, Tables 4 and 5). Actually, it is well known that the infrared bands due to the methylene stretching vibrations are sensitive to the physical state of the lipid and shift towards higher wavenumbers as the acyl chains become increasingly disordered. As shown in Table 4, the acyl chain disorder is higher for POPC than that of DMPC, in agreement with the presence of a double bond in the POPC acyl chains [51]. The fact that the wavenumber position of the band originating from the antisymmetric C–H stretching mode is quite high indicates that the acyl chains of MGDG and DGDG are highly disordered. In accordance with the values of the Raman intensity ratios $R_1 = I_{2930}/I_{2900}$ and $R_2 = I_{2900}/I_{2850}$, the acyl chains show a similar high degree of disorder for both MGDG and DGDG. The lateral cohesion of these chains increases from MGDG to DGDG and to the mixture. It can be assumed that the chain–chain coupling is stronger for DGDG than for MGDG in agreement with the difference of the mesophases formed in water, i.e., lamellar and inverse hexagonal phase, respectively. Nevertheless, the equimolar mixture appears to be more ordered with the stronger interchain coupling. The order parameter S_z obtained by ATR spectroscopy further confirms this result. The more negative value obtained for the mixture shows that the methylene groups are more parallel to the plane of the ATR crystal and, thus, the acyl chains are more vertical in accordance with a more ordered phase. Finally, the vibrational spectroscopy results converge towards little order for the phases adopted by pure MGDG or DGDG while more order is displayed in the phase adopted by the equimolar mixture of the two galactolipids. Because the lipid chains are highly disordered in monolayers or liquid-crystalline mesophases, the specific organization of galactolipids, especially for the mixture, should be due to the galactosyl headgroup interactions.

From our results and the abundant literature available on the interactions between oligosaccharides [57–60], the headgroup organization in monolayers and liquid-crystalline phases can be described and offers a better understanding of these interactions. In the lamellar phase determined for DGDG in excess water, the 54.9 Å bilayer thickness is close to the higher value found by Shipley et al. [40] for the corresponding *Pelargonium* galactolipid where the thickness of the bilayer varied from 44.8 to 54.0 Å (at 20 °C) for an increasing hydration level. This value is also quite comparable with that of 55.3 Å obtained by Sen et al. for DGDG extracted from bean leaves [41]. The reconstruction of the electron density (Fig. 8) was useful and has shown that the di-galactosyl headgroups are oriented parallel to the plane of the bilayer as observed by McDaniel [44]. We can then conclude that the decrease in the number of double bonds between DGDG extracted from leaves (C18:3) and seeds (C18:2) does not change the organization [61]. In monomolecular film the PM-IRRAS data (Fig. 4) have shown

that the di-galactosyl groups are oriented at 40° with respect to the normal to the interface. Thus, this observation underscores the ability of the DGDG headgroups to adopt a different orientation under the effect of the lateral compression. This organization of the headgroups adopted in monolayer as well as a greater proportion of saturated chains C16:0 compared to MGDG could explain that a lower mean molecular area is reached in the DGDG film (Fig. 2) which seems relatively thick compared to the other molecules (Fig. 3).

Concerning the MGDG inverse hexagonal phase, the obtained lattice parameter of 67.2 Å is clearly larger than values obtained in the work of Shipley et al. [40]. They found that distance between cylinder axes in the MGDG H_{II} phase (at 20 °C) varied from 52.5 to 60.5 Å for a dry and fully hydrated sample respectively, whereas the hydrated cylinder diameters changed from 17.4 to 29.8 Å. Our reconstruction of the electron density (Fig. 9) showed a specific behavior of mono-galactosyl headgroups. In fact, the MGDG headgroups are shifted on both sides from the experimental point C_{exp}. This shift between neighboring headgroups could be directly related to the AFM observations. The MGDG film displayed a roughness at 35 mN/m (Fig. 5) composed by protrusions that actually appeared from 25 mN/m (data not shown). Usually, this kind of observation is induced by either heterogeneity of the packing of the acyl chains or by the headgroup organization [34]. The first possibility can be excluded because both galactolipids are in fluid phase and in the case of DGDG, the images at 35 mN/m have shown uniform films although the chains were compressed to lower mean molecular area than MGDG. Therefore, the structures observed at 35 mN/m for MGDG should be due to an effect of galactosyl headgroups. According to the lateral size of the protrusions observed by AFM, the segregation concerns several molecules forming a labyrinth pattern whose lower width is around 50 nm. The difference in height between the background and the higher level is around 7 Å (Fig. 6). Increasing the surface pressure, the MGDG behavior in two dimensions seems to reveal a net tendency to the headgroup shifting and it may correspond to the beginning of the film curvature [62]. In addition to this topographic information, the orientation of oligosaccharide headgroups was estimated using PM-IRRAS spectra (Fig. 4), and we have deduced that the mono-galactosyl groups were oriented parallel to the interface. This conclusion is consistent with the large mean molecular area in the monomolecular film (Fig. 2) and also with the ellipsometric data that show a thinner film than other galactolipids (Fig. 3). At this stage, it is clear that the addition of only one galactosyl group in the polar head totally modifies the organization of the molecules in monolayers and in liquid-crystalline mesophases as well.

Regarding the equimolar mixture, previous studies on galactolipids have shown that *Ia3d* and *Pn3m* space groups are frequently observed and are correlated with the hydration level of the mesophase, i.e., low for *Ia3d* and high for *Pn3m* [63]. For example, the phase diagram of thylakoid membrane galactolipids exhibits a bicontinuous cubic phase which belongs to the *Ia3d* space group [6,64]. However, the structure of the phase formed by mixtures of the galactolipids MGDG and DGDG purified from the wheat seed has never been described. Our X-ray measurements for the equimolar mixture revealed a bicontinuous cubic phase which belongs to the *Im3m* space group. The lattice parameter is 202 Å. This space group was observed for synthetic β-D-galactosyl diacylglycerol with saturated acyl chains of 14 and 16 carbons [65]. By increasing the temperature, these systems first adopt a fluid lamellar phase then a first cubic phase *Pn3m* followed by an *Im3m* phase and finally by a H_{II} phase. This combination of cubic phases was also observed with shorter chain dialkyl PEs [62,66] but the lattice parameters were smaller than those of wheat galactolipids. For longer acyl chains (C18), these authors have shown that the transition goes directly from the L_{α} phase to the H_{II} phase. With similar chain length but with glucosyl headgroups, Turner et al. have shown the coexistence of *Ia3d* and *Pn3m* structures [67]. The presence of the *Im3m* space group could reveal specific interactions between headgroups of the molecules in the equimolar mixture of wheat MGDG and DGDG and in particular between galactosyl groups. This stabilization of the *Im3m* space group attributed to the strong interactions between galactosyl headgroups could lead to a slight decrease of the chain fluidity relative to the pure galactolipid phases as observed in the spectroscopic data mentioned above. This specific behavior in liquid-crystalline mesophase is also observed in monolayers using AFM. Actually, disconnected patches were observed with a height of 4 Å, which is smaller than the protrusions of 7 Å present in the MGDG LB film (Fig. 6). It is difficult to assign these domains to DGDG or MGDG. Nevertheless, the difference of topography could be related to changes of headgroup orientation induced by the interactions between both galactolipids. The PM-IRRAS spectra reveal these modifications (Fig. 4). We have deduced that, in the equimolar mixture, the monogalactosyl group of MGDG forces the digalactosyl group to adopt an orientation that is more parallel to the interface. The different orientations adopted by the galactosyl groups could be modulated by the hydrogen-bond network formed between headgroups and water molecules. This is supported by variations in the intensity and frequency of the water band on the PM-IRRAS spectra (around 1665 cm^{-1}) which is sensitive to variations in the optical properties and orientation of the interfacial water molecules. Whereas small differences are observed between MGDG and DGDG relating to the minimum attributed to water, a strong effect appeared for the equimolar mixture. Changes in the hydration are also highlighted for the C═O band on the PM-IRRAS spectra which is shifted to lower wavenumbers from MGDG (1736 cm^{-1}) to DGDG (1734 cm^{-1}) and to the equimolar MGDG/DGDG mixture (1729 cm^{-1}). Such a shift is generally related to hydrogen bonding of the carbonyl group with water molecules as shown for DMPC monolayer where the C═O band moved from 1737 to 1728 cm^{-1} as surface pressure decreased from 34 to 0.1 mN/m [68]. Moreover, it has been also shown for phospholipids in solution that the C═O band appears at 1740 cm^{-1} for free C═O groups, whereas it appears at 1726 cm^{-1} for hydrated C═O which form hydrogen bonds with water molecules [69,70]. In addition, a recent study has shown the formation of hydrogen bonds between the carbonyl groups of phosphatidylcholine and sugar molecules

[71]. In our case, the position of the C═O band should be sensitive to both the hydration of the carbonyl groups and the formation of hydrogen bonds between these groups and the galactosyl residues of the lipid headgroups. The fact that the lowest wavenumber position for the C═O band is obtained for the galactolipid mixture at 35 mN/m indicates that the galactolipid mixture displays higher hydration than the corresponding pure components even at high surface pressure. This higher hydration of the galactolipid mixture is also confirmed in the liquid-crystalline mesophase on the Raman spectra by the stronger intensity of the broad D_20 band between 2000 and 2800 cm^{-1} compared to the lipid bands between 2800 and 3050 cm^{-1} (Fig. 10). Finally, the low value of the C═O band for the equimolar mixture (1729 cm^{-1}) compared to the pure lipid suggests stronger hydrogen bonds between carbonyl groups and galactosyl residues. This could be explained by the reorientation of the polar headgroups observed in the mixture.

The results obtained in monolayers and in liquid-crystalline mesophases highlight specific galactosyl headgroup interactions in MGDG, DGDG and especially in the equimolar mixture. As outlined above, previous freeze-fracture studies on dry wheat seeds have permitted the observation of several types of lipid mesophases between the protein matrix and the starch granules. Lamellar, hexagonal and cubic phases were found around starch granules where the galactolipids are concentrated. In wheat endosperm, membrane lipids are composed by phospholipids and galactolipids. Most of the phospholipids are associated with the membranes of protein bodies and vacuoles and are characterized by a high level of N-acylphosphatidylethanolamines [72]. These lipids as MGDG form hexagonal phases in water [73]. During the programmed dehydration of endosperm in the last step of seed development, a lateral segregation of these non-lamellar lipids should occur, leading to the formation of non-lamellar phases between the protein matrix and starch granules. Such dehydration-induced transitions of the lamellar to hexagonal phases have been already observed in natural biomembranes [74,75]. The proportion between non-lamellar and lamellar lipids in endosperm membranes may control their phase behavior during dehydration of wheat seeds. This polymorphism may also be controlled by the kinetics of endosperm dehydration during the last step of seed development. Especially, the polymorphism of the lipids located at the interface between the starch granules and the protein matrix of the dried endosperm may control the extent of the packing of endosperm macromolecular compounds, i.e., storage proteins and starch. This packing determines the endosperm texture of wheat seeds, i.e., the allelic soft–hard variation of endosperm texture, an important physical characteristic that determines wheat milling properties and end-uses [12]. The unique behavior of MGDG and DGDG and especially of their mixture is probably important since close relationships between hexane-extractable galactolipids and wheat hardness have been highlighted [76]. The hexane extractability of polar lipids of wheat endosperm flour is probably related to the mesophase adopted by these lipids [11]. Finally, this polymorphism may also control the partition of puroindolines, a major lipid binding protein from wheat endosperm, onto the surface of starch granules, a phenomenon that discriminates hard and soft wheats [12,15]. The data obtained here open new perspectives to explore the relationships between endosperm texture and the phase behavior of polar lipids at the interface of the starch–protein matrix of wheat as other plant seeds.

Acknowledgments

We are grateful to T. Weiss and D. Durand for their help and advice regarding the experiments performed on the high brilliance ID2A at European Synchrotron Radiation Facility (Grenoble, France) and D43 at Laboratoire pour l′Utilisation du Rayonnement Electromagnétique (Orsay, France) synchrotron beamlines. European Synchrotron Radiation Facility is acknowledged for provision of beam time (SC1246). This work was supported by grants from Centre National de la Recherche Scientifique (doctoral fellowship for C. B.), Région Bretagne (postdoctoral fellowship for J. G.) and Centre de Coopération Interuniversitaire Franco-Québécoise (stay in Quebec of C. B.).

References

[1] T. Harder, K. Simons, Caveolae, DIGs, and the dynamics of sphingolipid–cholesterol microdomains, Curr. Opin. Cell Biol. 9 (1997) 534–542.
[2] T. Pali, G. Garab, L.I. Horvath, Z. Kota, Functional significance of the lipid–protein interface in photosynthetic membranes, Cell. Mol. Life Sci. 60 (2003) 1591–1606.
[3] B.D. Bruce, The role of lipids in plastid protein transport, Plant Mol. Biol. 38 (1998) 223–246.
[4] E. Marechal, M.A. Block, A.J. Dorne, R. Douce, J. Joyard, Lipid synthesis and metabolism in the plastid envelope, Physiol. Plant. 100 (1997) 65–77.
[5] J.L. Montillet, J.P. Agnel, M. Ponchet, F. Vailleau, D. Roby, C. Triantaphylidès, Lipoxygenase-mediated production of fatty acid hydraperoxydes is a specific signature of the hypersensitive reaction in plants, Plant Physiol. Biochem. 40 (2002) 633–639.
[6] I. Brentel, E. Selstam, G. Lindblom, Phase equilibria of mixtures of plant galactolipids: the formation of a bicontinuous cubic phase, Biochim. Biophys. Acta 812 (1985) 816–826.
[7] A.G. Lee, Membrane lipids: it's only a phase, Curr. Biol. 10 (2000) 377–380.
[8] M.J. Fishwick, A.J. Wright, Isolation and characterization of amyloplast envelope membranes from *Solanum tuberosum*, Phytochemistry 19 (1980) 55–59.
[9] E. Van den Brink-van der Laan, J.A. Killian, B.D. Kruijff, Nonbilayer lipids affect peripheral and integral membrane proteins via changes in the lateral pressure profile, Biochim. Biophys. Acta 1666 (2004) 275–288.
[10] K. Larsson, S. Puang-Ngern, The aqueous system of monogalactosyl diglycerides and digalactosyl diglycerides—Significance to the structure of the thylakoid membrane, in: L.Å. Appelqvist, C. Liljenberg (Eds.), Advances in the Biochemistry and Physiology of Plant Lipids, Elsevier/North Holland Biomedical press, 1979, pp. 27–33.
[11] D. Marion, L. Dubreil, P.J. Wilde, D.C. Clark, Lipids, lipid–protein interactions and the quality of baked cereal products, in: R.J. Hamer, R.C. Hoseney (Eds.), In Interactions: the keys to cereal quality, AACC, St-Paul, MN, 1998, pp. 131–167.
[12] K.M. Turnbull, S. Rahman, Endosperm texture in wheat, J. Cereal Sci. 36 (2002) 327–337.
[13] A. Al Saleh, D. Marion, D.J. Gallant, Microstructure of mealy and vitreous wheat endosperms (*Triticum durum* L.) with special emphasis on location and polymorphic behavior of lipids, Food Microstruct. 5 (1986) 131–140.
[14] J.B. Ohm, O.K. Chung, NIR transmittance estimation of free lipid content and its glycolipid and digalactosyldiglyceride contents using wheat flour lipid extracts, Cereal Chem. 77 (2000) 556–559.
[15] J.P. Douliez, T. Michon, K. Elmorjani, D. Marion, Structure, biological and

technological functions of lipid transfer proteins and indolines, the major lipid binding proteins from cereal kernels, J. Cereal Sci. 32 (2000) 1–20.
[16] L. Dubreil, V. Vié, S. Beaufils, D. Marion, A. Renault, Aggregation of puroindoline in phospholipid monolayers spread at the air–liquid interface, Biophys. J. 85 (2003) 2650–2660.
[17] S.G. Sprague, L.A. Staehelin, Effects of reconstitution method on the structural organization of isolated chloroplast membrane lipids, Biochim. Biophys. Acta 777 (1984) 306–322.
[18] J. Folch, M. Lees, G.H. Sloane-Stanley, A simple method for the isolation and purification of total lipids from animal tissues, J. Biol. Chem. 226 (1956) 497–509.
[19] J.H. Gil, J. Hong, J.C. Choe, Y.H. Kim, Analysis of fatty acyl groups of diacyl galactolipid molecular species by HPLC/ESI-MS with in-source fragmentation, Bull. Korean Chem. Soc. 24 (2003) 1163–1168.
[20] Y.H. Kim, J.H. Gil, J. Hong, J.S. Yoo, Tandem mass spectrometric analysis of fatty acyl groups of galactolipid molecular species from wheat flour, Microchem. J. 68 (2001) 143–155.
[21] B. Berge, A. Renault, Ellipsometry study of 2D crystallization of 1-alcohol monolayers at the water surface, Europhys. Lett. 21 (1993) 773–777.
[22] R.M.A. Azzam, N.M. Bashara, Ellipsometry and Polarized Light, Elsevier/North Holland, Amsterdam, 1977, p. 340.
[23] D. Blaudez, T. Buffeteau, J.C. Cornut, B. Desbat, N. Escafre, M. Pézolet, J.M. Turlet, Polarization-modulated FT-IR spectroscopy of a spread monolayer at the air/water interface, Appl. Spectrosc. 47 (1993) 869–874.
[24] D. Blaudez, J.-M. Turlet, Dufourcq, D. Bard, T. Buffeteau, B. Desbat, Investigations at the air/water interface using polarization modulation IR spectroscopy, J. Chem. Soc., Faraday Trans. 92 (1996) 525–530.
[25] T. Narayanan, O. Diat, P. Bösecke, SAXS and USAXS on the high brilliance beamline at the ESRF, Nucl. Instrum. Methods Phys. Res., A 467–468 (2001) 1005–1009.
[26] N. Hauet, F. Artzner, F. Bouchery, C. Grabielle-Madelmont, I. Cloutiery, G. Keller, P. Lesieur, D. Durand, M. Paternostre, Interaction between artificial membranes and enflurane, a general volatile anesthetic: DPPC–enflurane interaction, Biophys. J. 84 (2003) 3123–3137.
[27] C. Valéry, F. Artzner, B. Robert, T. Gulick, G. Keller, C. Gabrielle-Madelmont, M.L. Torres, R. Cherif-Cheikh, M. Paternostre, Self-association process of a peptide in solution: from b-sheet filaments to large embedded nanotubes, Biophys. J. 86 (2004) 2484–2501.
[28] T.C. Huang, H. Toraya, T.N. Blanton, Y. Wu, X-ray powder diffraction analysis of silver behenate, a possible low-angle diffraction standard, J. Appl. Crystallogr. 26 (1993) 180–184.
[29] T.N. Blanton, T.C. Huang, H. Toraya, C.R. Hubbard, S.B. Robie, D. Louër, H.E. Göbel, G. Will, R. Gilles, T. Raferty, JCPDS—International Centre for diffraction data round robin study of silver behenate. A possible low-angle X-ray diffraction calibration standard, Powder Diffraction 10 (1995) 91–95.
[30] R. Zantl, Flüssigkristalle aus DNA und kationischen lipidmembranen, Ph.D. Thesis. Technische Universität, Munich. Germany (2001).
[31] D.G. Cameron, J.K. Kauppinen, D.J. Moffat, H.H. Mantsch, Precision in condensed phase vibrational spectroscopy, Appl. Spectrosc. 36 (1982) 245–250.
[32] R.A. Demel, W.S.M.G.v. Kessel, L.L.M.v. Deenen, The properties of polyunsaturated lecithins in monolayers and liposomes and the interactions of these lecithins with cholesterol, Biochim. Biophys. Acta 266 (1972) 26–40.
[33] D.G. Bishop, J.R. Kenrick, J.H. Bayston, A.S. Macpherson, S.R. Johns, Monolayers properties of chloroplast lipids, Biochim. Biophys. Acta 602 (1980) 248–259.
[34] V. Vié, N.V. Mau, E. Lesniewska, J.P. Goudonnet, F. Heitz, C.L. Grimellec, Distribution of ganglioside GM1 between two-component, two-phase phosphatidylcholine monolayers, Langmuir 14 (1998) 4574–4583.
[35] J. Gallant, R.M. Leblanc, Purification of galactolipids by high-performance liquid chromatography for monolayer and Langmuir–Blodgett film studies, J. Chromatogr., A 542 (1991) 307–316.
[36] P. Tancrede, G. Chauvette, R.M. Leblanc, General method for the purification of lipids for surface pressure studies. Application to monogalactosyldiglyceride, J. Chromatogr., A 207 (1981) 387–393.
[37] K. Tamada, H. Minamikawa, M. Hato, Phase transition in glycolipid monolayers induced by attractions between oligosaccharide head groups, Langmuir 12 (1996) 1666–1674.
[38] J.A. de Feijter, J. Benjamins, F.A. Veer, Ellipsometry as a tool to study the adsorption behavior of synthetic and biopolymers at the air–water interfaces, Biopolymers 17 (1978) 1759–1772.
[39] D. Ducharme, J.J. Max, C. Salesse, R.M. Leblanc, Ellipsometric study of the physical state of phosphatidylcholines at the air–water interface, J. Phys. Chem. 94 (1990) 1925–1932.
[40] C.G. Shipley, J.P. Green, B.W. Nichols, The phase behavior of monogalactosyl, digalactosyl, and sulphoquinovosyl diglycerides, Biochim. Biophys. Acta 311 (1973) 531–544.
[41] A. Sen, W.P. Williams, P.J. Quinn, The structure and thermotropic properties of pure 1,2-diacylgalactosylglycerols in aqueous systems, Biochim. Biophys. Acta 663 (1981) 380–389.
[42] A. Tardieu, V. Luzzati, F.C. Reman, Structure and polymorphism of the hydrocarbon chains of lipids: a study of lecithin–water phases, J. Mol. Biol. 75 (1973) 711–733.
[43] P.E. Harper, D.A. Mannock, R.N.A.H. Lewis, R.N. McElhaney, S.M. Gruner, X-ray diffraction structures of some phosphatidylethanolamine lamellar and inverted hexagonal phases, Biophys. J. 81 (2001) 2693–2706.
[44] R.V. McDaniel, Neutron diffraction studies of digalactosyldiacylglycerol, Biochim. Biophys. Acta 940 (1988) 158–164.
[45] C. Valéry, M. Paternostre, B. Robert, T. Gulik-Krzywicki, T. Narayanan, J.-C. Dedieu, G. Keller, M.-L. Torres, R. Cherif-Cheikh, P. Calvo, F. Artzner, Biomimetic organization: octapeptide self-assembly into nanotubes of viral capsid-like dimension, Proc. Natl. Acad. Sci. U. S. A. 100 (2003) 10258–10262.
[46] V. Luzzati, A. Tardieu, T. Gulik-Krzywicki, E. Rivas, F. Reiss-Husson, Structure of the cubic phases of lipid–water systems, Nature 7 (1968) 485–488.
[47] L. Rilfors, P.-O. Eriksson, G. Arvidson, G. Lindblomf, Relationship between three-dimensional arrays of "lipidic particles" and bicontinuous cubic lipid phases, Biochemistry 25 (1986) 7702–771 I.
[48] J.M. Seddon, R.H. Templer, Polymorphism of lipid–water systems, in: R. Lipowsky, E. Sackmann (Eds.), Structure and Dynamics of Membranes, vol. 1, Elsevier/North Holland, Amsterdam, 1995, pp. 98–160.
[49] Y. Rançon, J. Charvolin, Epitaxial relationships during phase transformations in a lyotropic liquid crystal, J. Phys. Chem. 92 (1988) 2646–2651.
[50] S. Kutsumizu, T. Ichikawa, M. Yamada, S. Nojima, S. Yano, Phase transitions of 4′-n-Hexacosyloxy-3′-nitrobiphenyl-4-carboxylic acid (ANBC-26): two types of thermotropic cubic phases, J. Phys. Chem., B 104 (2000) 10196–10205.
[51] C. Lee, C.D. Bain, Raman spectra of planar supported lipid bilayers, Biochim. Biophys. Acta 1711 (2005) 59–71.
[52] B.P. Gaber, W.L. Peticolas, On the quantitative interpretation of biomembrane structure by Raman spectroscopy, Biochim. Biophys. Acta 465 (1977) 260–274.
[53] R.G. Snyder, J.R. Scherer, B.P. Gaber, Effects of chain packing and chain mobility on the Raman spectra of biomembranes, Biochim. Biophys. Acta 601 (1980) 47–53.
[54] M.R. Bunow, I.W. Levin, Comment on the carbon-hydrogen stretching region of vibrational Raman spectra of phospholipids, Biochim. Biophys. Acta 487 (1977) 388–394.
[55] C. Huang, J.T. Mason, I.W. Levin, Raman spectroscopic study of saturated mixed-chain phosphatidylcholine multilamellar dispersions, Biochemistry 22 (1983) 2775–2780.
[56] F. Picard, T. Buffeteau, B. Desbat, M. Auger, M. Pézolet, Quantitative orientation measurements in thin lipid films by attenuated total reflection infrared spectroscopy, Biophys. J. 76 (1999) 539–551.
[57] K. Matsuura, H. Kitakouji, R. Oda, Y. Morimoto, H. Asano, H. Ishida, M. Kiso, K. Kitajima, K. Kobayashi, Selective expansion of the GM3 glycolipid monolayer induced by carbohydrate–carbohydrate interaction with Gg3 trisaccharide-bearing glycoconjugate polystyrene at the air–water interface, Langmuir 18 (2002) 6940–6945.
[58] V. Vill, R. Hashi, Carbohydrate liquid crystals: structure–property relationship of thermotropic and lyotropic glycolipids, Curr. Opin. Colloid Interface Sci. 7 (2002) 395–409.
[59] A.V. Popova, D.K. Hincha, Intermolecular interactions in dry and rehydrated

pure and mixed bilayers of phosphatidylcholine and digalactosyldiacylglycerol: a Fourier transform infrared spectroscopy study, Biophys. J. 85 (2003) 1682–1690.
[60] K. Shinoda, A. Carlsson, B. Lindman, On the importance of hydroxyl groups in the polar headgroup of nonionic surfactants and membrane lipids, Adv. Colloid Interface Sci. 64 (1996) 253–271.
[61] A.V. Popova, D.K. Hincha, Effects of the sugar headgroups of a glycoglycerolipid on the phase behavior of phospholipid model membranes in the dry state, Glycobiology 15 (2005) 1150–1155.
[62] J.M. Seddon, Structure of the inverted hexagonal (HII) phase, and non-lamellar transitions of lipids, Biochim. Biophys. Acta 1031 (1990) 1–69.
[63] G. Lindblom, L. Rilfors, Cubic phases and isotropic structures formed by membrane lipids: possible biological relevance, Biochim. Biophys. Acta 988 (1989) 221–256.
[64] E. Rivas, V. Luzzati, Polymorphisme des lipides polaires et des galactolipids de chloroplastes de maïs en présence d'eau. J. Mol. Biol. 41 (1969) 261–275.
[65] D.A. Mannock, P.E. Harper, S.M. Gruner, R.N. McElhaney, The physical properties of glycosyl diacylglycerols. Calorimetric, X-ray diffraction and Fourier transform spectroscopic studies of a homologous series of 1,2-di-O-acyl-3-O-(b-D-galactopyranosyl)-sn-glycerols, Chem. Phys. Lipids 111 (2001) 139–161.
[66] J.M. Seddon, J.L. Hogan, N.A. Warrender, E. Pebay-Peroula, Structural studies of phospholipid cubic phases, Prog. Colloid & Polym. Sci. 81 (1990) 189–197.
[67] D.C. Turner, Z.G. Wang, S.M. Gruner, D.A. Mannock, R.N. McElhaney, Structural study of the inverted cubic alkyl-β-D-glucopyranosyl-rac-glycerol, J. Phys. II France 2 (1992) 2039–2063.
[68] J. Saccani, Réalisation de systèmes membranaires modèles et étude de leur organisation par microscopie à l'angle de Brewster, spectroscopie PM-IRRAS et dichroïsme circulaire vibrationnel, Thèse de doctorat de l'université Bordeaux 1 (2003).
[69] A. Blume, W. Huebner, G. Messner, Fourier transform infrared spectroscopy of $^{13}C{=}O$-labeled phospholipids hydrogen bonding to carbonyl groups, Biochemistry 27 (1988) 8239–8249.
[70] R.N. Lewis, R.N. McElhaney, W. Pohle, H.H. Mantsch, Components of the carbonyl stretching band in the infrared spectra of hydrated 1,2-diacylglycerolipid bilayers: a reevaluation, Biophys. J. 67 (1994) 2367–2375.
[71] C. Cacela, D.K. Hincha, Low amounts of sucrose are sufficient to depress the phase transition temperature of dry phosphatidylcholine, but not for lyoprotection of liposomes, Biophys. J. 90 (2006) 2831–2842.
[72] K.D. Hargin, W.R. Morrison, The distribution of acyl lipids in the germ, aleurone, starch and non-starch endosperm of four wheat flour varieties, J. Sci. Food Agric. 31 (1980) 877–888.
[73] S. Akoka, C. Tellier, C.L. Roux, D. Marion, A phosphorus magnetic resonance spectroscopy and a differential scanning calorimetry study of the physical properties of N-acylphosphatidylethanolamines in aqueous dispersions, Chem. Phys. Lipids 46 (1988) 43–50.
[74] L.M. Crowe, J.H. Crowe, Hydration-dependent hexagonal phase lipid in a biological membrane, Arch. Biochem. Biophys. 217 (1982) 582–587.
[75] W.J. Gordon-Kamm, P.L. Steponkus, Lamellar to hexagonal II phase transitions in the plasma membranes of isolated protoplasts after freeze-induced dehydration, Proc. Natl. Acad. Sci. U. S. A. 81 (1984) 6373–6377.
[76] J.B. Ohm, O.K. Chung, Relationships of free lipids with quality factors in hard winter wheat flours, Cereal Chem. 79 (2002) 274–278.